

Microscopic driving theory with non-hypothetical congested steady state: model and empirical verification

Jun-fang Tian^{*1}, Martin Treiber², Bin Jia³, Wen-yi Zhang³

¹*Institute of Systems Engineering, College of Management and Economics, Tianjin University, No. 92 Weijin Road, Nankai District, Tianjin 300072, China*

²*Technische Universität Dresden, Institute for Transport & Economics, Würzburger Str. 35, D-01062 Dresden, Germany*

³*MOE Key Laboratory for Urban Transportation Complex Systems Theory and Technology, Beijing Jiaotong University, Beijing, 100044, China*

The essential distinction between the fundamental diagram approach and three-phase theory is the existence of the unique space-gap-speed relationship. In order to verify this relationship, empirical data are analyzed with the following findings: (1) linear relationship between the actual space gap and speed can be identified when the speed difference between vehicles approximates zero; (2) vehicles accelerate or decelerate around the desired space gap most of the time. To explain these phenomena, we propose that, in homogeneous congested traffic flow, the space gap between two vehicles will oscillate around the desired space gap in the noiseless limit. This assumption is formulated in terms of a cellular automaton. Simulations under periodic and open boundary conditions reproduce the empirical findings of three-phase theory. Finally, the model is calibrated and validated. All verification results are acceptable and better than that of previous studies.

Key words: cellular automaton; three-phase traffic flow; fundamental diagram; safe time gap

1. Introduction

With the rapid development of urbanization, traffic congestion becomes one of the most serious problems that undermine the operational efficiency of modern cities. In order to understand the mechanism of traffic congestion, many models and analysis have been carried out to explain the empirical findings (see the reviews: Haight, 1963; Whitham, 1974; Leutzbach, 1987; Chowdhury, 2000; Helbing, 2001; Nagatani, 2002; Jia et al. 2007; Kerner, 2004, 2009; Treiber and Kesting, 2013). Generally speaking, these models can be classified into the fundamental diagram approach and models consistent with three-phase theory.

Originated from Greenshields (1935), the fundamental diagram permeates all levels of traffic flow models and is one of the basic research technics of empirical data. The fundamental diagram is the idealized form of the

*Corresponding author.

E-mail address:jftian@tju.edu.cn

1 flow-density curve in traffic flow, which goes through the origin and has at least one maximum. It describes the
2 theoretical relationship between density and flow in the stationary homogeneous traffic, i.e., the steady state of
3 identical driver-vehicle units (Treiber and Kesting, 2013). In the last century, almost all traffic flow models belong to
4 the fundamental diagram approach. In microscopic models, the fundamental diagram is linked to the steady states of
5 car-following (CF) or cellular automaton (CA) models. For example, in the Optimal Velocity Model (OV model) by
6 Bando et al. (1995), the fundamental diagram corresponds to the optimal velocity function itself. In the
7 Nagel-Schreckenberg cellular automaton model (NaSch model), it could be derived in terms of the steady state in the
8 deterministic limit (Nagel and Schreckenberg, 1992). In macroscopic or mesoscopic models, it has been directly
9 applied (e.g. the LWR theory (Lighthill and Whitham, 1955; Richards, 1956)) or incorporated into the momentum
10 equation (e.g. the PW theory (Payne, 1979)).

11 The majority of models within the fundamental diagram approach belongs to the two-phase models (Lighthill
12 and Whitham, 1955; Richards, 1956; Herman et al., 1959; Payne 1979; Gipps, 1981; Nagel and Schreckenberg, 1992;
13 Daganzo, 1994; Bando et al., 1995; Krauss et al., 1997; Treiber et al., 2000; Aw and Rascle, 2000; Newell, 2002; Tang,
14 2005)), which refers to the free flow phase (F) and the jammed phase (J). The phase transitions involved are the
15 transition from free flow to jams (F→J transition) and the transition from jam to free flow (J→F transition). The
16 fundamental diagram approach explains the jam formation mainly by excess demand, i.e., the traffic inflow exceeds
17 the static capacity defined by the maximum of the fundamental diagram. Additionally, instabilities of traffic flow,
18 which are caused by finite speed adaption times (due to finite accelerations) or reactiontimes, can lead to jam
19 formation even before static capacity is reached. For the detailed discussion of stability, one can refer to Treiber and
20 Kesting (2013), Kesting and Treiber (2008).

21 Based on the long-term empirical analysis, Kerner (2004, 2009) argues that two-phase models could not
22 reproduce the empirical features of traffic breakdown as well as the further development of the related congested
23 region properly. Therefore, the three-phase theory is introduced distinguishing (1) free traffic flow, (2) synchronized
24 flow, and (3) wide moving jams. The fundamental hypothesis of the three-phase theory is that the hypothetical steady
25 states of the synchronized flow cover a two-dimensional region in the flow-density plane. In other words, there is no
26 fundamental diagram of traffic flow. Over the time, many models within the framework of three-phase theory are
27 proposed (Kerner et al., 2002, 2011; Kerner, 2012; Kerner and Klenov 2002, 2003, 2006; Lee et al., 2004; Jiang and
28 Wu, 2003, 2005; Tian et al., 2009; Gao et al., 2007, 2009; Davis, 2004). In order to improve readability, we have made
29 a brief introduction of three-phase theory in the appendix.

30 It should be noted that there are models within the fundamental diagram approach that could reproduce the
31 three-phase theory, such as the Brake Light cellular automaton Model (BLM (Knospe, 2000)), the Speed Adaption
32 Models (SAMs (Kerner and Klenov, 2006)), and the Average Space Gap cellular automaton Model (ASGM (Tian et
33 al., 2012a, 2012b)). However, some of these models have been criticized by proponents of three-phase theory. BLM
34 has been criticized because its congested patterns are inconsistent with the empirical findings (Kerner et al., 2002).
35 SAMs are not able to reproduce the observed local synchronized patterns (LSPs) as well as some of empirical features
36 of synchronized flow between wide moving jams within general patterns (GPs) (Kerner and Klenov, 2006). However,
37 these criticisms cannot be applied to the ASGM which can describe the LSPs and GPs very well.

38 Although this paper is motivated by the inconsistency between fundamental diagram approach and three-phase
39 theory, the purpose is not to discuss their controversies. Instead, this paper aims to describe the driver behavior by a
40 cellular automaton containing explicit oscillations around the steady-state in the noiseless limit thereby reproducing
41 the major observational aspects of three-phase theory. Moreover, empirical calibration and validation results in a
42 higher accuracy than that of previously investigated models (Brockfeld et al., 2005; Wagner et al., 2010). To these
43 ends, Section 2 analyses the US-101 trajectory datasets on a single freeway lane, away from lane changes and the
44 influence of bottlenecks. Section 3 proposes a cellular automaton model that incorporates this assumption. Empirical
45 findings of three-phase theory are simulated and discussed in Section 4. Section 5 is devoted to calibrating and
46 validating the model to the I-80 detector data. The concluding Section 6 gives a summary and a discussion.

1
2
3
4
5
6
7
8
9
10
11
12
13
14
15
16
17
18
19
20
21
22
23
24
25
26
27
28
29
30
31
32
33
34
35
36
37
38
39

2. Empirical data analysis

The essential distinction between the fundamental diagram approach and the three-phase theory is whether the fundamental diagram exists. Three-phase theory supposes the existence of a two-dimensional region in the density-flow plane or, equivalently, in the gap-speed plane. Drivers can make an arbitrary choice in the space gap within a certain region. The fundamental diagram approach assumes the existence of a unique gap-speed relationship. For example, the Intelligent Driver Model (IDM) presumes the following relationship (Treiber et al., 2000):

$$s^*(v, \Delta v) = s_0 + vT + \frac{v\Delta v}{2\sqrt{ab}} \tag{1}$$

Here, s^* is the desired gap. The meaning and typical values of the IDM parameters are shown in Tab.1. The relationship between the space gap s and speed v in the steady state is $s=s_0+vT$, which is also assumed in other car following models such as Newell's model (Newell, 2002). Thus, the validation of the relation $s=s_0+vT$ contributes to resolving these controversies between the fundamental diagram approach and three-phase theory. However, it is impossible to validate this relationship by the real traffic data directly, since real traffic flow is always away from the steady state, at least, to some extent. Nevertheless, Equation (1) indicates that we can validate this relationship, if the speed difference between vehicles is approximately zero. Therefore, in order to exclude the influence of the speed difference Δv , we only analyze the empirical data with $|\Delta v| \leq \Delta v_c$. The value of Δv_c should be able to neglect the influence of Δv and, nevertheless, make the empirical sample size large enough. Assuming $|\Delta v| \leq \Delta v_c$, we have $s^* \approx s_0 + vT$. A suitable value for Δv_c is 0.1 m/s.

Table 1
Model Parameters and values of IDM (Treiber and Kesting, 2013).

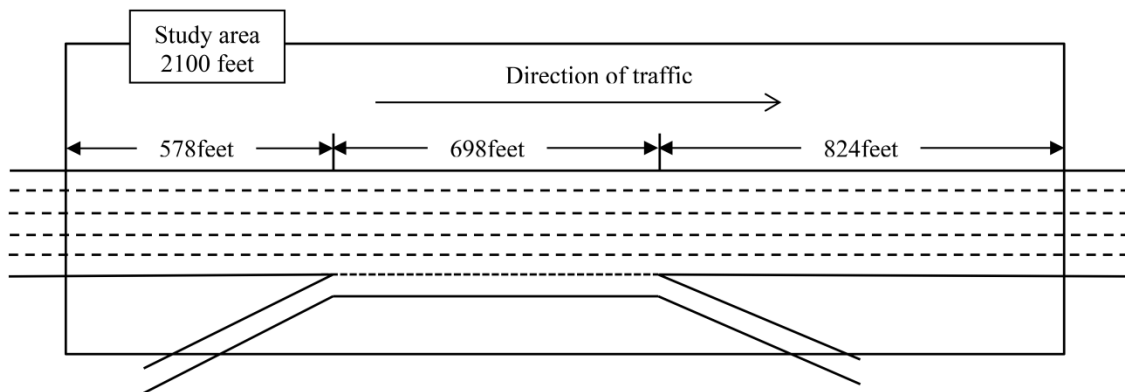
Parameter (unit)	Typical value	Reasonable range
Safe time gap $T(s)$	1.5	0.9~3
Minimum gap $s_0(m)$	2	1~5
Acceleration $a (m/s^2)$	1.4	0.3~3
Comfortable deceleration $b (m/s^2)$	2.0	0.5~3

Next, the US-101 trajectory data sets of the Next Generation Simulation Community (NGSIM, 2006) are applied to validate $s=s_0+vT$. These data were collected on a 640m segment on the south-bound direction of US 101 (Hollywood Freeway) in Los Angeles, California on June 15th, 2005. The data were detected from 7:50 a.m. to 8:05 a.m., 8:05 a.m. to 8:20 a.m., and 8:20 a.m. to 8:35 a.m. During the data collection period, the California Highway Patrol's Computer Aided Dispatch (CHP CAD) system was monitored. No traffic incidents were recorded during the morning of June 15th on US-101 within the study area or on any upstream/downstream sections likely influencing traffic in the study area. Fig.1 provides a schematic illustration of the location for the vehicle trajectory datasets. There are five mainline lines throughout the section, and an auxiliary lane is present through a portion of the corridor between the on-ramp and off-ramp. In order to minimize the impact of bottlenecks on traffic flow, only the leftmost lane is analyzed. The following criteria are used to filter suitable trajectories from the empirical data:

1. The vehicle's leading car could not change lanes during the whole period,
2. the absolute value of the vehicle speed difference to the leader is smaller than 0.1m/s,
3. there are at least 100 data points for the selected vehicle, i.e. a trajectory duration of 10 seconds or more,
4. the space headway should be shorter than 76m (250ft). Otherwise, it is likely that there is no interaction (Bham and Benekohal, 2004).

After applying these criteria, 323 out of 1226 vehicle trajectories were included in the analysis, see Tab.2. The optimal values of T and s_0 for each vehicle were estimated by the linear regression analysis. Some results are shown in

1 Figs.2 and 3. The linear relationship between the actual space gap s and speed v are identified when the speed
 2 difference approaches zero. Figs.2 and 3 also illustrate that vehicles will not keep uniform speeds although the actual
 3 space gap s approximates desired space gap s^* calculated by $s^* = s_0 + vT$, and speed difference Δv approximates zero.
 4 This means that, even if the stimulus vanish, i.e., $\Delta v \rightarrow 0$ and $s \rightarrow s^*$, the vehicles accelerate or decelerate most of the
 5 time. While this could possibly be explained by the drivers' anticipation or finite reaction time, we make the following
 6 assumptions to explain this phenomenon from another perspective: *In homogeneous congested traffic flow and in the*
 7 *noiseless limit, the space gap will oscillate around the (speed dependent) desired value rather than maintain this value.*
 8 In this perspective, no steady states exist in the homogeneous congested traffic flow. This is different from the
 9 fundamental diagram approach or the three-phase theory, which admit the existence of definite steady states or a
 10 multitude of steady states, respectively. In this perspective, even if the actual space gap equals the desired space gap
 11 and the speed difference is approximately zero, vehicles will accelerate or decelerate in an oscillatory way. It should
 12 be noted that many car following models considered very small fluctuations around the desired space gap, i.e.
 13 acceleration noise. However, it is impossible that the acceleration noise is responsible for the high observed values of
 14 accelerations and decelerations depicted in Fig.3.
 15

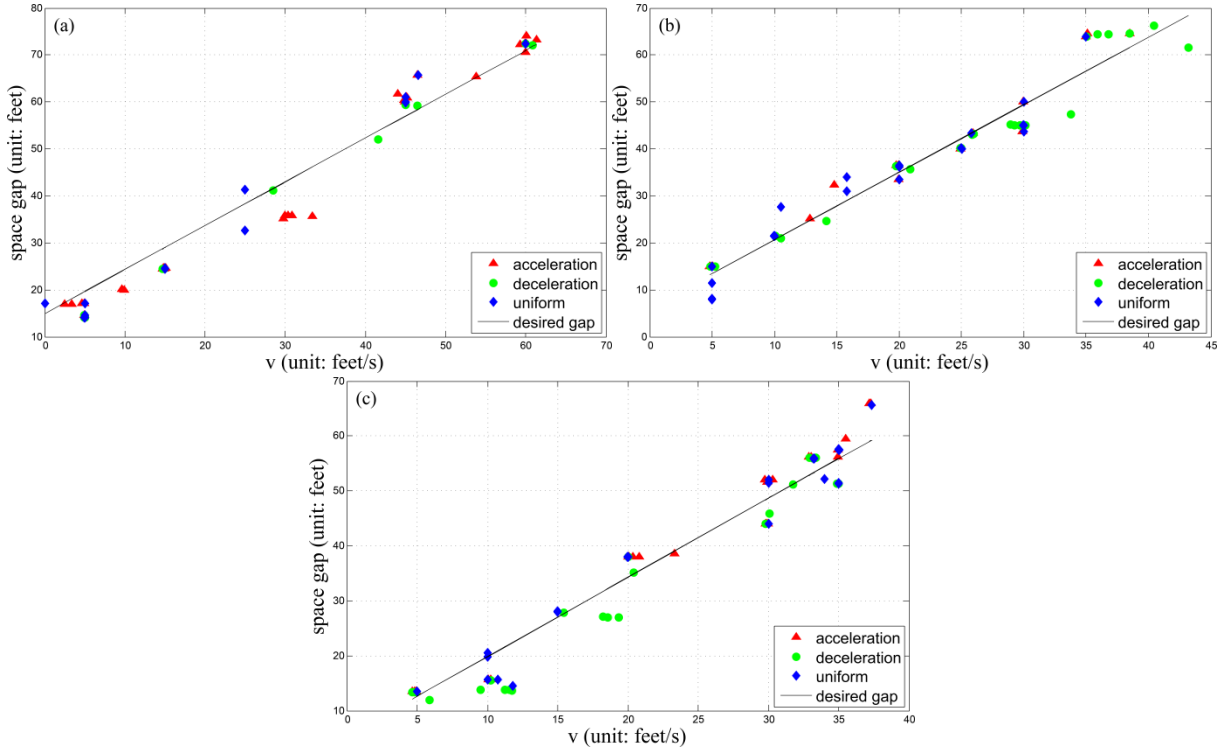


16
 17 **Fig. 1.** The sketch of US-101 study area.
 18

19 **Table 2**
 20 Overview of F-Tests of the linear relationship between space gap and speed.

Time interval	Number of simples available before filtering	Number of simples available before testing for significance	Number of simples available after testing for significance	
			s_0	lower 95% confidence bounds of s_0 greater than zero
07:50am-08:05am	430	84	84	74
08:05am-08:20am	410	98	97	78
08:20am-08:35am	386	141	139	113
Total	1226	323	320	265

21
 22



1

2

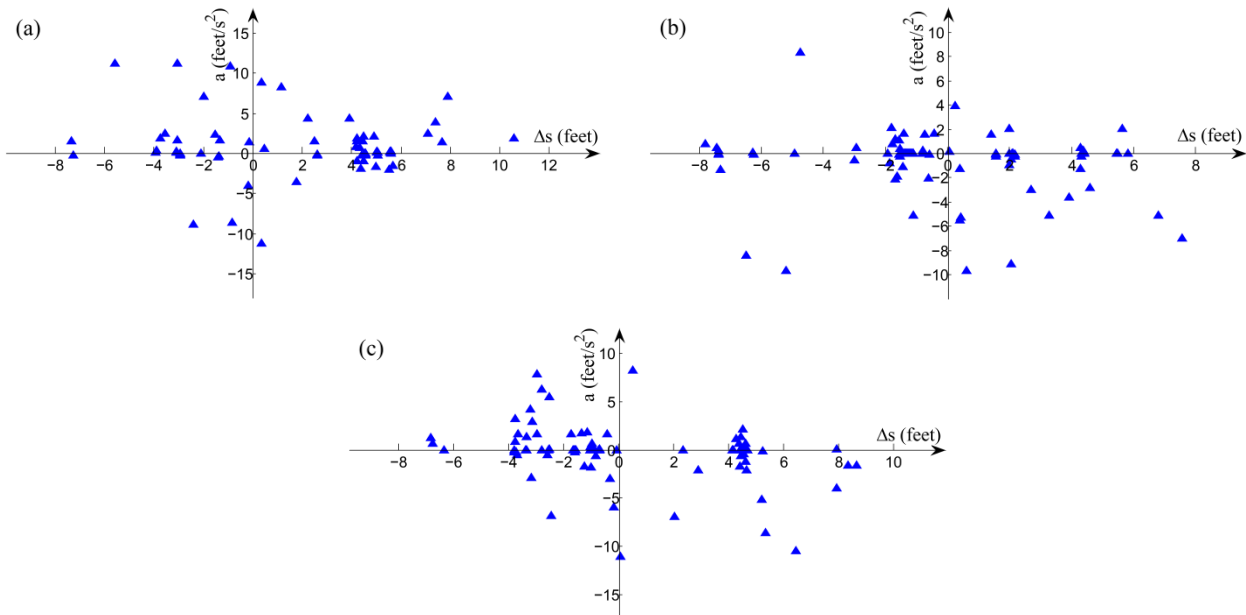
3

4

5

6

Fig.2. Linear regression analysis for the space gap as a function of the speed. (a-c) are single-vehicle data taken from different detecting time intervals 7:50 a.m. to 8:05 a.m., 8:05 a.m. to 8:20 a.m., and 8:20 a.m. to 8:35 a.m., respectively. Speed, acceleration and space gap are the instantaneous speed, acceleration and space gap respectively, which are taken from the raw record data without any processing. If the acceleration or deceleration is less than $0.1m/s^2$, we assume a steady-state situation.



7

8

9

10

11

12

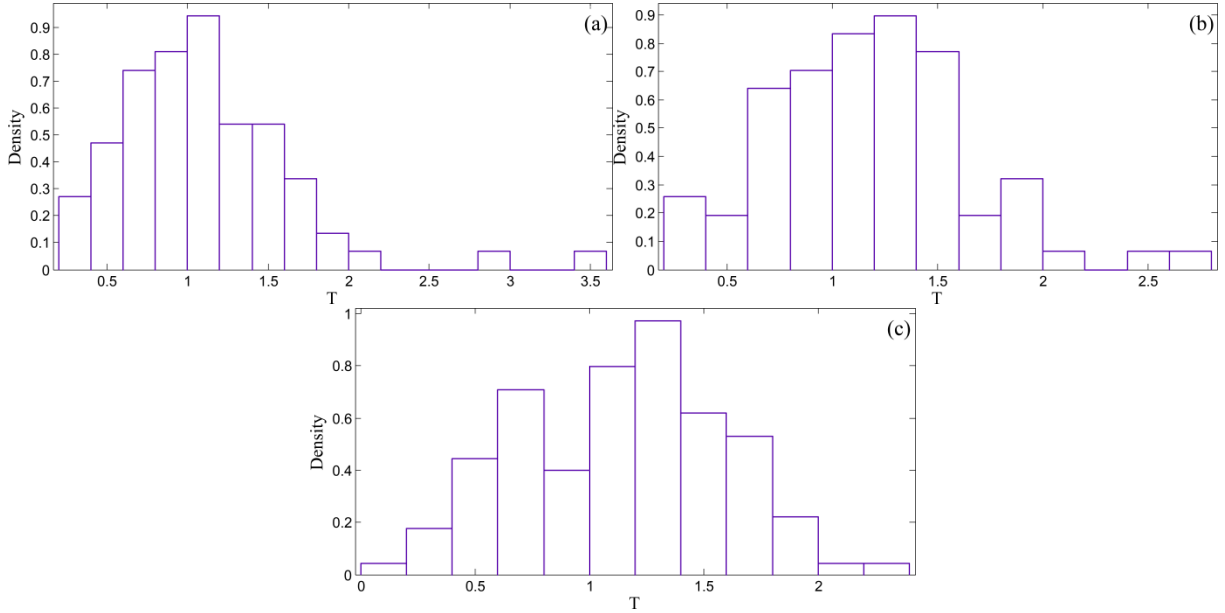
13

14

Fig.3. The accelerations corresponding to Fig. 2(a-c), respectively. $\Delta s = s - s_0 - vT$ denotes the deviation from the steady-state gap.

F-Tests for significance of the linear relationship at a level of 5% are also performed. The results are shown in Tab.2 and Fig.4. Tab. 2 shows that almost all data indicate the existence of the linear relationship, although some values of s_0 are less than zero. If the data with the lower 95% confidence bound of s_0 less than zero are excluded, there remain still 265 samples (82%).

1



2

3

Fig.4. Histograms of the safe time gaps. (a-c) correspond to the detecting time intervals 7:50 a.m. to 8:05 a.m., 8:05 a.m. to 8:20 a.m., and 8:20 a.m. to 8:35 a.m., respectively.

6

7

3. The new model

8

We propose a new cellular automaton model based on the above assumption, i.e., vehicles' space gap will oscillate around the desired space gap in the homogeneous congested traffic flow in the noiseless limit. The main mechanisms incorporating this assumption are embodied in the randomization process of vehicles. The parallel-update rules are as follows.

12

1. Determination of the randomization parameter $p_n(t+1)$ and deceleration extent Δv :

13

$$p_n(t+1) = \begin{cases} p_a & : \text{ if } d_n^{eff}(t) < d_n^*(t) \\ p_b & : \text{ if } v_n(t) = 0 \text{ and } t_n^{st}(t) \geq t_c \\ p_c & : \text{ in all other cases} \end{cases} \quad (2)$$

14

$$\Delta v(t+1) = \begin{cases} b_{defens} & : \text{ if } d_n^{eff}(t) < d_n^*(t) \\ 1 & : \text{ in all other cases} \end{cases} \quad (3)$$

15

2. Acceleration:

16

$$v_n(t+1) = \min(v_n(t) + 1, v_{max})$$

17

3. Deceleration:

18

$$v_n(t+1) = \min(d_n^{eff}(t), v_n(t+1))$$

19

4. Randomization with probability $p_n(t+1)$:

20

$$\text{if } (rand() < p_n(t+1)) \text{ then } v_n(t+1) = \max(v_n(t+1) - \Delta v(t+1), 0)$$

21

5. Determination of $t_n^{st}(t+1)$:

22

$$\text{if } (v_n(t+1) = 0) \text{ then } t_n^{st}(t+1) = t_n^{st}(t) + 1$$

23

$$\text{if } (v_n(t+1) > 0) \text{ then } t_n^{st}(t+1) = 0$$

6. Car motion:

$$x_n(t+1) = x_n(t) + v_n(t+1)$$

Here, $d_n(t)$ is the space gap between vehicle n and its preceding vehicle $n+1$, $d_n(t) = x_{n+1}(t) - x_n(t) - L_{veh}$, $x_n(t)$ is the position of vehicle n (here vehicle $n+1$ precedes vehicle n), and L_{veh} is the length of the vehicle. Furthermore, $v_n(t)$ is the speed of the vehicle n , v_{max} is the maximum speed, $d_n^*(t) = Tv_n(t)$ is the effective desired space gap between vehicle n and $n+1$, and T is the effective safe time gap between vehicle n and $n+1$ at the steady state, and $d_n^{eff}(t) = d_n(t) + \max(v_{anti}(t) - g_{safety}, 0)$ is the effective gap. In this definition, $v_{anti} = \min(d_{n+1}(t), v_{n+1}(t) + 1, v_{max})$ is the expected speed of the preceding vehicle in the next time step, and g_{safety} the parameter to control the effectiveness of the anticipation. Accidents are avoided only if the constraint $g_{safety} \geq b_{defens}$ is satisfied. The speed anticipation effect is considered in order to reproduce the real time headway distribution, which has a cut off at the small time headway less than one second (Neubert et al., 1999). $t_n^{st}(t)$ denotes the time since the last stop for standing vehicles, while $t_n^{st}(t) = 0$ for moving vehicles.

The basis of the new model is the rule set of the NaSch model with randomization parameter p_c to which a slow-to-start rule and the effective desired space gap $d_n^*(t)$ have been added. The slow-to-start effect is characterized by an increase of the randomization parameter from p_c to p_b ($> p_c$), which is the element to realize the transition from synchronized flow to wide moving jams. The new model assumes the driver tends to keep the effective gap no smaller than $d_n^*(t)$, otherwise the driver will become defensive. The actual behavioral change is characterized by increasing the spontaneous braking probability from p_c to p_a . Moreover, the associated deceleration will change from 1 to b_{defens} (≥ 1). This effect is the factor to reproduce the transition from free flow to synchronized flow in the new model.

In the following, the steady states of the new model are analyzed in the unperturbed, noiseless limit. For microscopic traffic flow models, the steady state requires that the model parameters are the same for all drivers and vehicles. In that case, the steady state is characterized by the following two conditions (Treiber and Kesting, 2013):

1) *Homogeneous traffic*: All vehicles move at the same speed and keep the same gap behind their respective leaders.

2) *No accelerations*: all vehicles keep a constant speed.

Since the mechanisms associated with the hypothetical congested steady state analysis are all embodied in the randomization process, the noiseless limit should be taken as $p_a = 1, p_c = 0, p_b = 0$ or $p_a = 1, p_c = 1, p_b = 1$. However, all vehicles will keep a constant speed no matter how far distance between vehicles in the latter case, which is obviously unrealistic. Thus, we consider the former. According to the model rules, if $d^{eff} / T \geq v_{max}$, all vehicles will move with v_{max} ; if $d^{eff} / T < v_{max}$, all vehicles' speed will take turns to change simultaneously over time between $\max(v - b_{defens}, 0)$ and v , where $v \in [d^{eff} / T, \min(v_{max}, d^{eff})]$ and $\max(v - 1, 0) < d^{eff} / T$. This means that there are no steady states of congested traffic in the new model. Instead, the space gaps oscillate around the desired gap, i.e., fluctuations are caused by the internal randomness of the drivers, not (only) by the driver heterogeneity, which is consistent with the empirical findings by Wagner (2012). Thus, this model is named as the cellular automaton model with non-hypothetical congested steady state (NH model). Finally, we note that by modifying the acceleration

rule of the NH model as follows, we obtain a cellular automaton model within the fundamental diagram approach:

$$\text{if } d_n^{\text{eff}}(t) > d_n^*(t) \text{ then : } v_n(t+1) = \min(v_n(t) + 1, v_{\max}) \quad (4)$$

4 Simulation investigation

In this section, simulations are carried out on a road of length $L_{\text{road}} = 1000L_{\text{cell}}$. Both the cell length and vehicle length are set as $7.5m$. One time step corresponds to $1s$ in reality. During the simulations, the first 50000 time steps are discarded to let the transients die out. The parameters are shown in Tab.3.

Table 3

Model parameters of NH model.

Parameters	L_{cell}	L_{veh}	v_{\max}	T	b_{defens}	p_a	p_b	p_c	g_{safety}	t_c
Units	m	L_{cell}	L_{cell}/s	s	L_{cell}/s^2	-	-	-	L_{cell}	s
Value	7.5	1	5	1.8	1	0.95	0.55	0.1	2	8

4.1. Periodic boundary condition

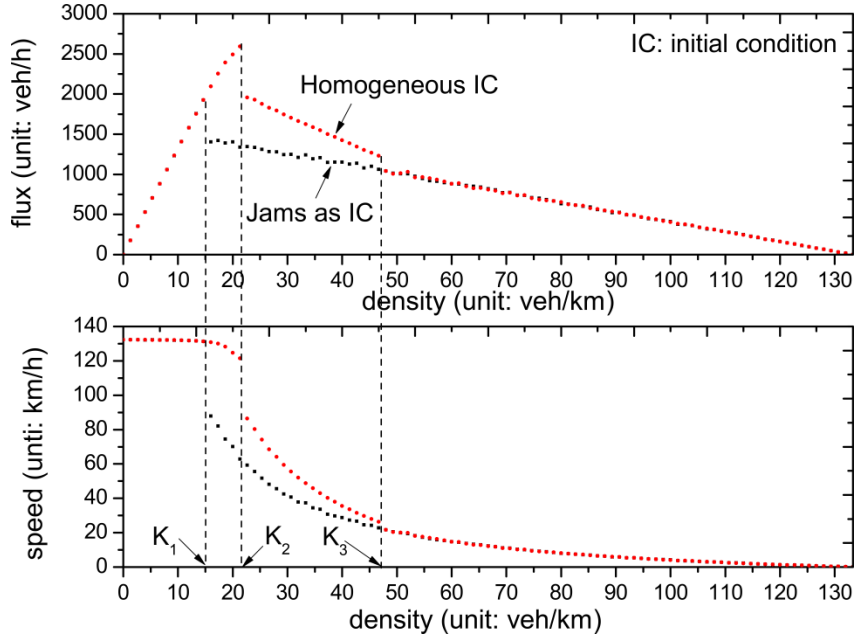
Periodic boundary conditions reflect a ring road, i.e., the first vehicle N is connected to the last vehicle 1 by the boundary conditions

$$v_{N+1} = v_1, \quad d_{N+1} = x_1 + L_{\text{road}} - x_n - L_{\text{veh}} \quad (5)$$

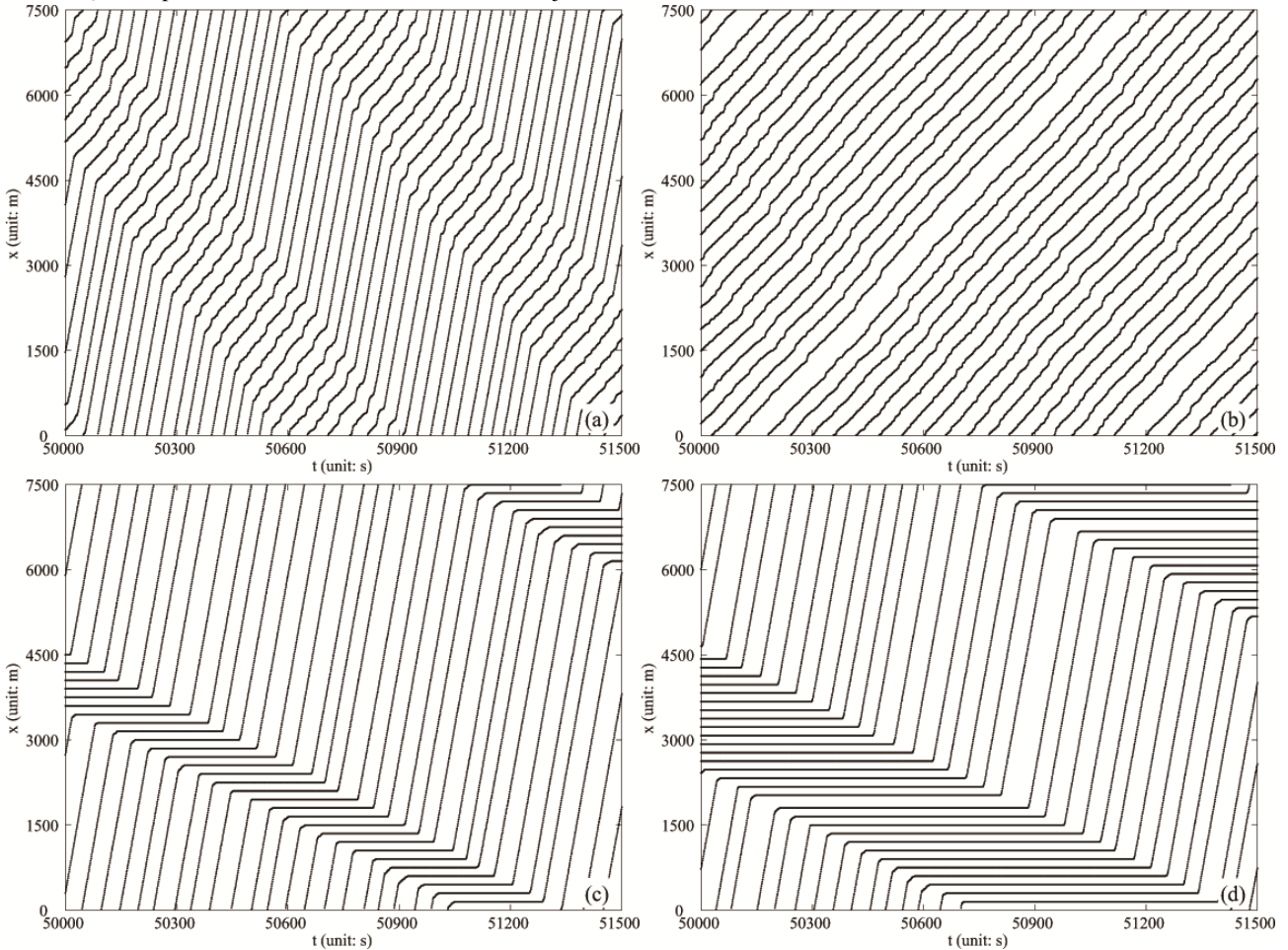
Figure 5 shows the macroscopic flow-density diagram by plotting the time-averaged flux f (vehicles per hour) at a given location over the global density K . Since the number N of vehicles and thus the global density $K = N/L_{\text{road}}$ is fixed, each data point corresponds to an individual simulation.

One can see that there are two branches in the density region $K_1 < K < K_3$: the upper branch is obtained from the initially homogeneous distribution of traffic whereas the lower starts from a wide moving jam. Therefore, three traffic phases and two first order transitions (the transitions from free flow to synchronized flow (F→S) and from synchronized flow to wide moving jams (S→J)) are clearly distinguished, exhibiting a typical double Z-characteristic structure predicted by the three-phase traffic flow theory. Moreover, when the density increases ($K_2 < K < K_3$), the flux begins to decrease and the synchronized flow starts to emerge in the free flow when the initially state is homogeneous traffic (Fig.6(a),(b)). While the initially wide moving jams traffic will evolve to the state that wide moving jams and free flow coexist (Fig.6(c),(d)).

Next, we distinguish the synchronized flow and the wide moving jam phases with single traffic data by the flow interruption effect (see Appendix). We obtained the data by setting a virtual detector on the road. Fig.7 shows the sketch of virtual detector on the road. The detector measures the numbers and speeds of the vehicles that pass it in the aggregation time interval $60s$. Since the state of each cell is known, we can tell whether the cell is occupied by the vehicle. Therefore, if the detector location is within the wide moving jam, there is no vehicle passing it. Both the number and speed of vehicles are zero. It is different from the real detector, which cannot measure speed if the number of vehicles is zero because one cannot tell apart stopped traffic from an empty road. The interruption effect can be clearly identified in the Figs.8(a),(b). Before and after the wide moving jam has passed the detector, many vehicles traversed the detector. But within the jam, no vehicles traversed the detector, and the speed within the jam is zero. This means that the traffic flow is discontinuous within the moving jam, i.e., this moving jam is associated with the wide moving jam phase. The flow interruption does not occur in the Figs.8(c),(d). Thus, this is associated with the synchronized flow phase.



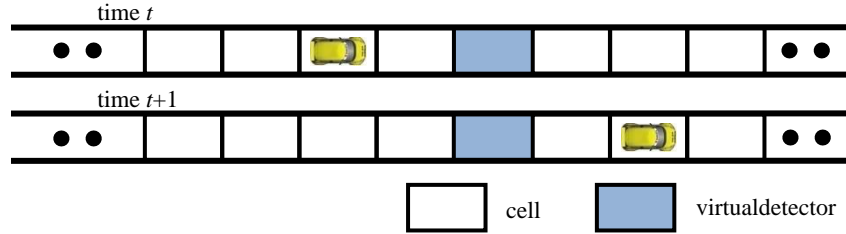
1
 2 **Fig.5.** Flow-density diagram of NH model. "Homogeneous IC" represents the initially homogenous distribution of traffic, and "Jams as IC"
 3 IC" represents the initially wide moving jam distribution of traffic. The upper lines between K_2 and K_3 in the flux-density and
 4 speed-density plots, respectively, correspond to a mixture of coexisting free traffic and synchronized phases, while the lower line between
 5 K_1 and K_3 corresponds to a coexistence of free traffic and jams.



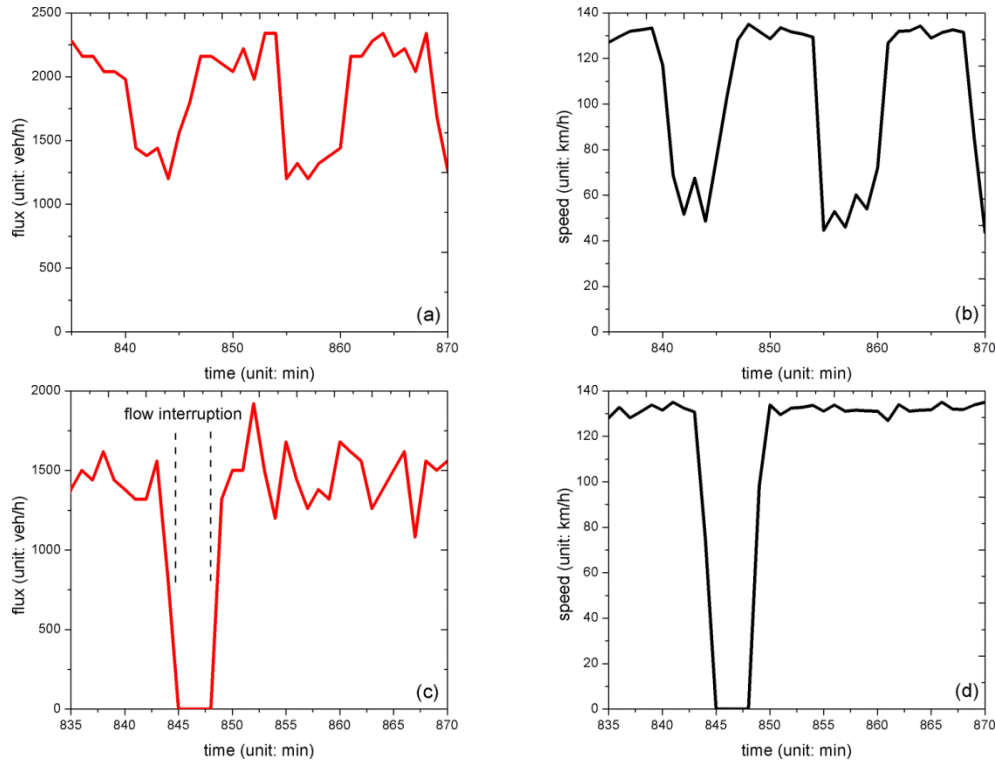
6

7

1 **Fig.6.** Trajectories of every 20th vehicle of the NH model, (a) $k=27$, (b) $k=47$, (c) $k=27$, (d) $k=47$ (unit: *veh/km*). (a),(b) Starting from
 2 homogeneous initial state. (c),(d) Starting from a wide moving jam initial state. The horizontal direction (from left to right) is time and the
 3 vertical direction (from down to up) is space.
 4



5 **Fig.7.** The sketch of a virtual detector.
 6
 7



8
 9 **Fig.8.** (a), (c) The 1 min average flux. (b),(d) The 1 min average speed. (a),(b) stating from homogenous initial state responding to
 10 Fig.6(a). (c),(d) starting from a wide moving jam initial state responding to Fig.6(c).
 11
 12

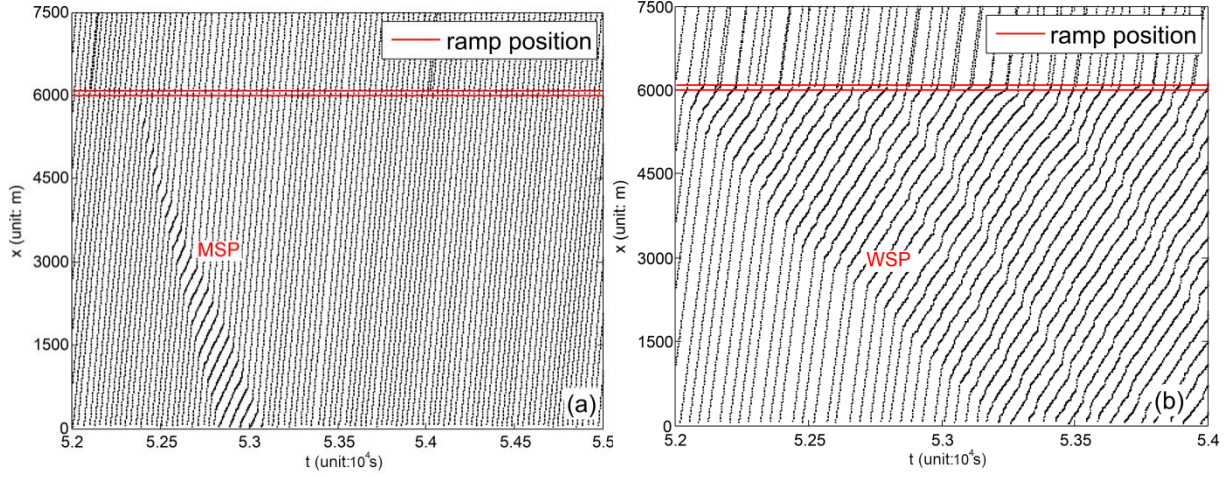
13 **4.2. Open boundary condition**

14 The traffic patterns that emerge near an on-ramp are studied under open boundary condition. The vehicles drive
 15 from left to right. The left-most cell corresponds to $x=1$. The position of the left-most vehicle is x_{last} and that of the
 16 right-most vehicle is x_{lead} . At each time step, if $x_{last} > v_{max}$, a new vehicle with speed v_{max} will be injected to the position
 17 $\min(x_{last} - v_{max}, v_{max})$ with probability $q_{in}/3600$ where q_{in} is the traffic flow entering the main road in units of vehicles
 18 per hour. At the right boundary, the leading vehicle moves without any hindrance. If $x_{lead} > L_{road}$, the leading vehicle will
 19 be removed and the following vehicle becomes the leader.

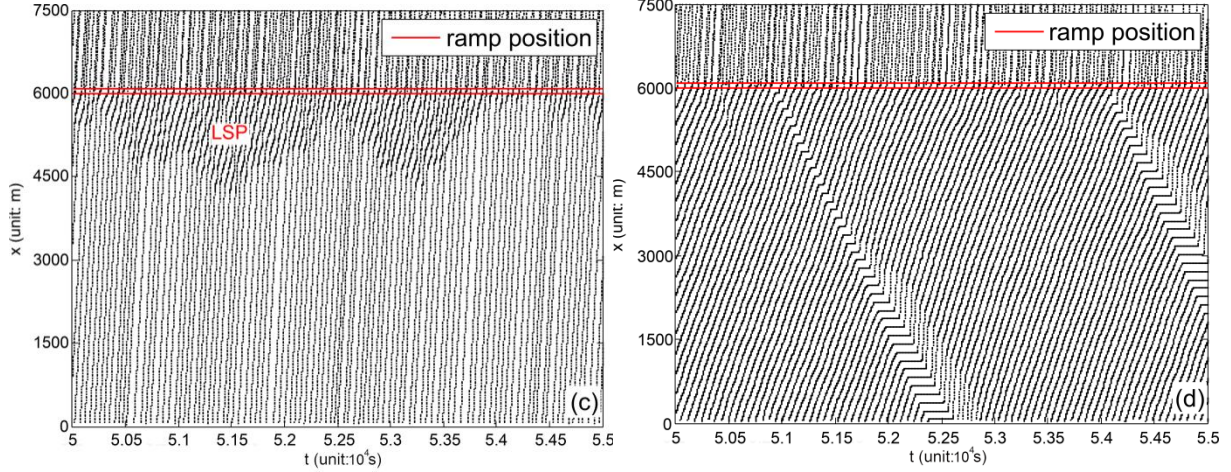
20 We adopt a simple method to model the on-ramp, which is similar to that of Treiber et al. (2006). Assuming the
 21 position of the on-ramp is x_{on} , a region $[x_{on}, x_{on} + L_{ramp}]$ is selected as the inserting area of the vehicle from on-ramp. At
 22 each time step, we find out the longest gap in this region. If the gap is large enough for a vehicle, then a new vehicle

1 will be inserted at the cell in the middle of the gap with probability $q_{in}/3600$ and q_{on} is the traffic flow from the
 2 on-ramp. The speed of the inserted vehicle is set as the speed of its preceding vehicle, and the stop time is set to zero.
 3 The parameters are set as $x_{on}=0.8L_{road}$ and $L_{ramp}=10L_{cell}$.
 4

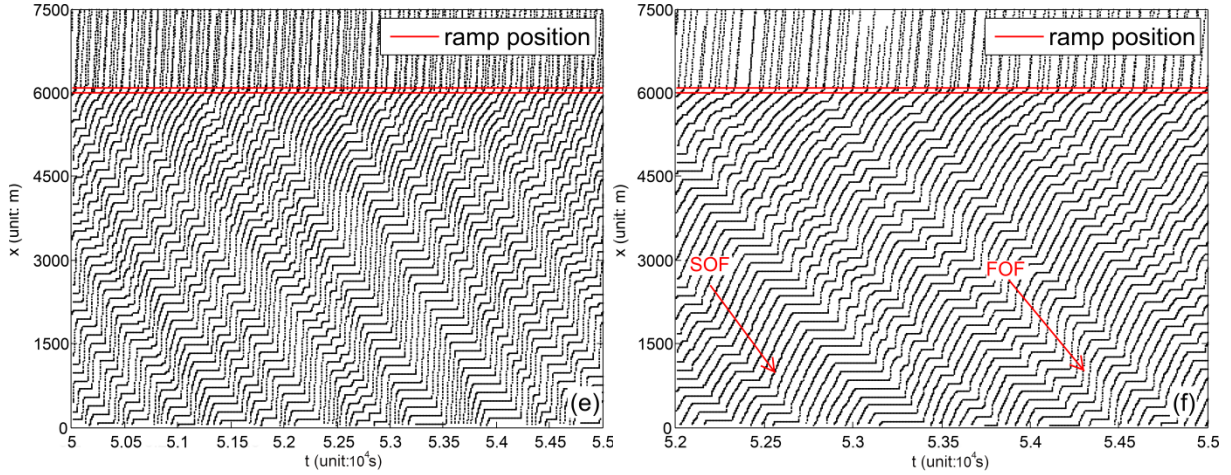
5



6



7



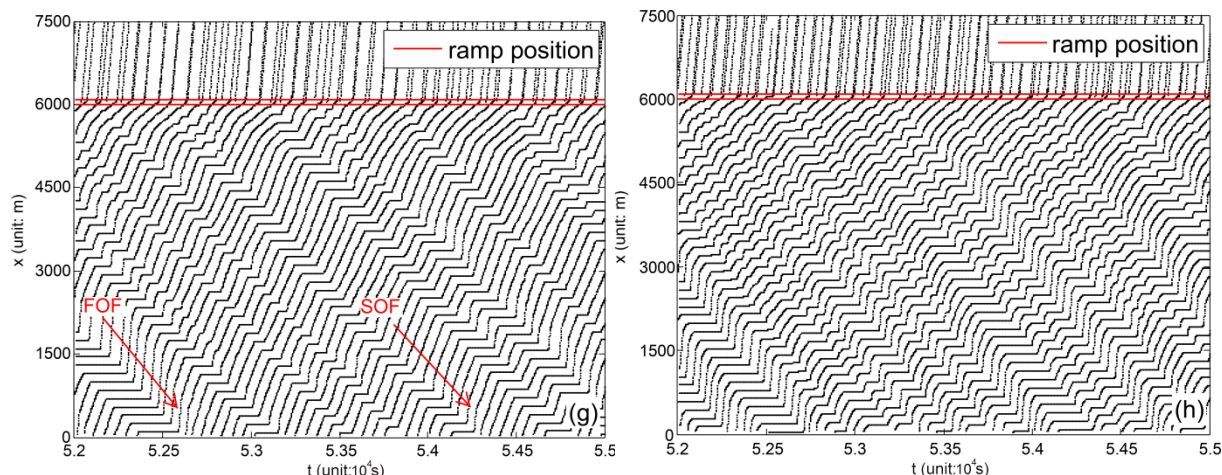


Fig.9. Trajectories of every 20th vehicle of the NH model. (a) $q_{in}=2339, q_{on}=19$ (MSP), (b) $q_{in}=1728, q_{on}=968$ (WSP), (c) $q_{in}=1440, q_{on}=823$ (LSP), (d) $q_{in}=1134, q_{on}=1123$ (DGP), (e) $q_{in}=920, q_{on}=1304$ (GP), (f) $q_{in}=931, q_{on}=1304$ (GP), (g) $q_{in}=933, q_{on}=1011$ (GP), (h) $q_{in}=907, q_{on}=1410$ (GP) (unit: veh/h). The horizontal direction (from left to right) is time and the vertical direction (from down to up) is space. (f) $p_b=0.5$, (g) $p_b=0.55, T=1.6, g_{safety}=b_{defens}=2$, (h) the acceleration rule is according to equation (4). 'SOF' and 'FOF' represent the synchronized outflow and free outflow of wide moving jams, respectively.

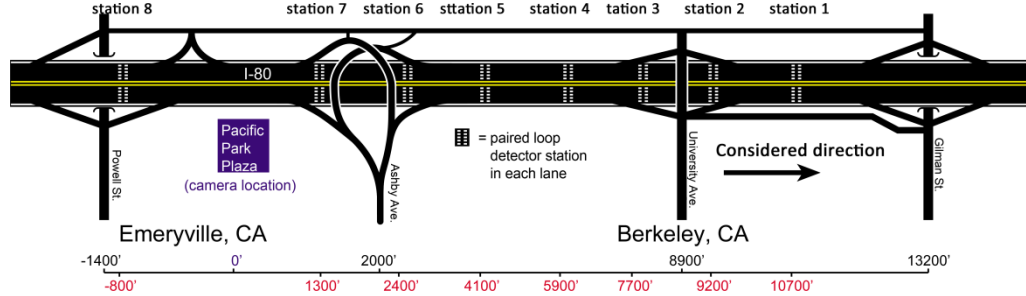
In Fig.9(a), the spatial-temporal features of the congested pattern named moving synchronized flow (MSP) reproduced are shown (see the empirical figure 7.6 in Kerner (2009)). In this pattern, synchronized traffic flow spontaneously emerges in the free flow. Fig.9(b) exhibits the widening synchronized flow (WSP, see the empirical figure 7.4 in Kerner (2009)). For this pattern, wide moving jams do not emerge in synchronized flow. The downstream front of WSP is fixed at the on-ramp and the upstream front of WSP propagates upstream continuously over time. In Fig.9(c), both the downstream and the upstream front of synchronized flow are fixed at the on-ramp, thus, it belongs to the local synchronized pattern (LSP). Moreover, the width of LSP in the longitudinal direction changes over time, which is in accordance with empirical observations (see the empirical figure 7.2 in Kerner (2009)). Fig.9(d) shows the dissolving General Patterns (DGP) in which just one wide moving jam emerges in the synchronized flow. Fig.9(e) shows the spatial-temporal features of General Pattern (GP). Only free outflow exists in the downstream of wide moving jams in GP, which has been criticized by the three-phase theory. However, it can be easily improved if we decrease the slow-to-start probability p_b or adjust the values of T and b_{defens} , see Fig.9(f),(g). Thus, all the above simulation results are well consistent with the well-known results of the three-phase traffic theory. However, if the acceleration rule is revised as equation (4), the synchronized outflow cannot be reproduced any more.

In Fig. 9(a) and (d), one could obtain the propagation velocity of the downstream MSP front is nearly -26.8km/h and the propagation velocity of the downstream jam front is nearly -13km/h which is about half that of the downstream MSP front. This is better than in most three-phase models which often have propagation velocities as negative as -40km/h or even more negative.

5. Empirical validation

In order to validate NH model, comparing the simulating data with the empirical data is necessary. The datasets presented by NGSIM are from double loop detectors between Powell Street and Gilman Avenue on Interstate 80 (I-80) in Emeryville, California, see Fig.10. The I-80 is a five-lane freeway. The data were collected through Freeway Performance Measurement System (PeMS) project, which was conducted by the Department of Electrical Engineering and Computer Sciences at the University of California, at Berkeley, with the cooperation of California Department of Transportation. Available data from six detector stations (Stations 1, 3, 4, 5, 6 and 7) were provided in this data set.

1 Each detector station contains two detectors per lane. This data set provides 30-second processed, loop detector data.
 2 Speed (unit: *feet/s*), volume (unit: *number*) and occupancy (unit: *percentage*) at each detector for the 30-second time
 3 step are presented at each detector in each lane. The NH model will be calibrated with the data of Thursday, 07 April
 4 2005 and then validated with the data of other five days.



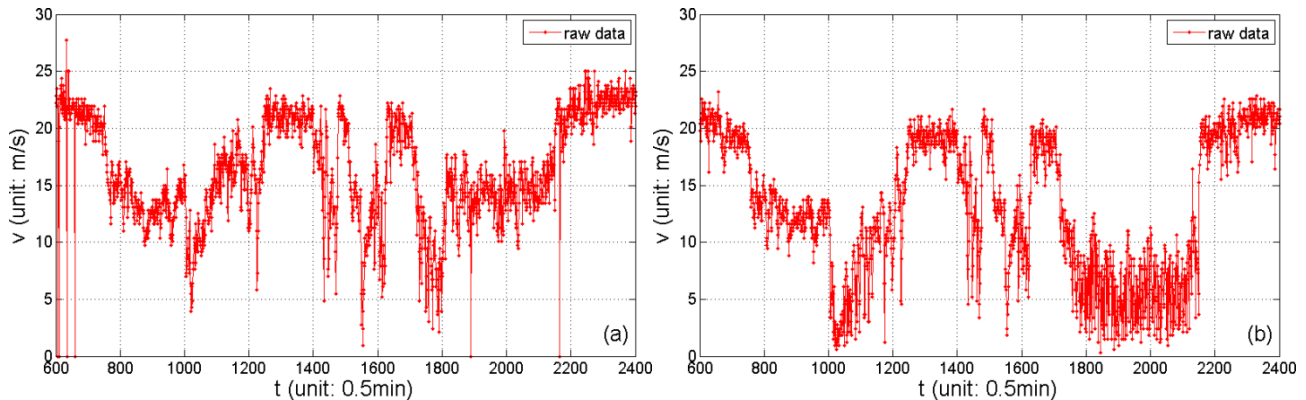
7
8
9 **Fig.10.** The sketch of I-80 near Berkeley.

10 As in the investigation of Brockfeld et al. (2005), we average the speed and flux data over the N lanes to obtain
 11 effective single lane speeds v_{ave}^i and fluxes f_{ave}^i as follows:

12
$$v_{ave}^i = \sum_{j=1}^N w_{ij} v_{ij}^{emp}, w_{ij} = \frac{f_{ij}^{emp}}{\sum_{j'=1}^N f_{ij'}^{emp}}, \quad (5)$$

13
$$f_{ave}^i = \frac{1}{N} \sum_{j=1}^N f_{ij}^{emp} \quad (6)$$

14 where f_{ij}^{emp} and v_{ij}^{emp} are the empirical flux and speed of lane j detected by the station i . Empirical fluxes
 15 $f_{ij}^{emp} = n_{ij}^{emp} / 30$ (unit: *veh/s*) are defined by dividing the number n_{ij}^{emp} of vehicles passing in each time interval
 16 30s over station i on lane j by this interval. Since NH model is a single-lane model, this avoids the additional
 17 complexity of lane-change rules needed to perform multi-lane simulation. Free traffic and synchronized flow can be
 18 identified in Fig.11 (a-e), which shows the time series of speed for each lane at Station 5 on Thursday, 07 April 2005.
 19 Fig.11(f) is the average speed (v_{ave}^5) data on the station 5, derived from Equation (5). Comparing with Fig.11(a-e),
 20 Fig.11(f) is capable of reflecting the same traffic dynamics around Station 5. Thus, this method is useful to test
 21 whether the NH model can describe the real traffic flow patterns.



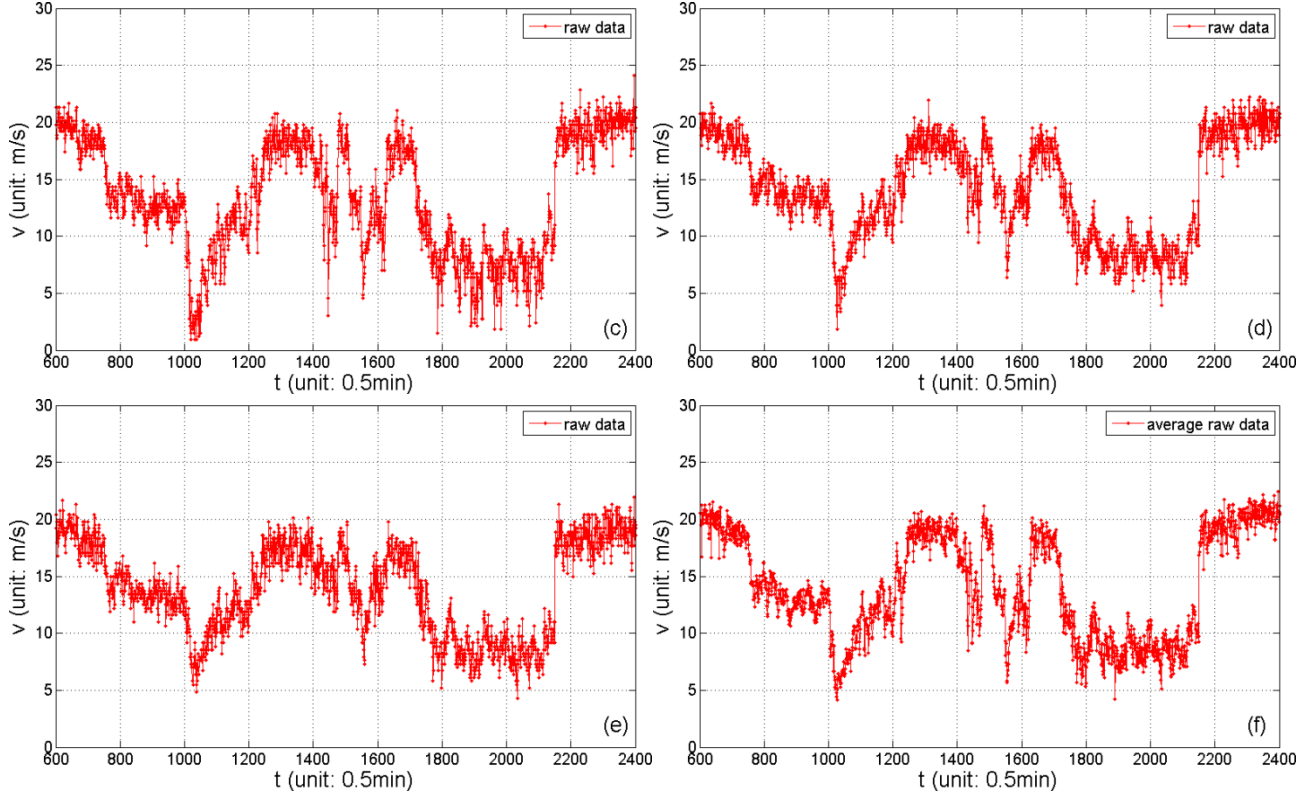


Fig.11. Real Time series of speed at Station 5 on Thu, 07 Apr 2005. (a-e) correspond to the real speed series lane 1 to lane 5 detected by station 5. (f) is the real lane average speed series calculated by Equation (5).

5.1. Simulation setup

The vehicles are generated at inflow Station 6. To insert new vehicles, the in-flowing open boundary condition in section 4.2 is applied. The position of station 6 is set at the left-most cell. At each time step, if $x_{last} > v_{max}$, a new vehicle with speed v_{max} will be injected to the position $\min(x_{last} - v_{max}, v_{max})$ with probability $q_{in} = f_{ave}^6$.

To regulate the outflow, the limit speed region closely downstream of Station 4 is defined, which starts from the position of Station 4, and ends with the length $L_{sl}=50m$, i.e., the speed limit region is located at $[1067, 1117]m$. In the speed limit region, a dynamic speed limit is applied, which equals the speed v_{ave}^4 that Station 4 measured. Since the CA models require an integer value for the speed limit, we converted the value to $\lfloor v_{ave}^4 / L_{cell} + 1 \rfloor$, where $\lfloor x \rfloor$ denotes the maximum integer that is not bigger than x . The simulation ends at 1117m.

5.2. Goodness-of-fit measures

Theil's inequality coefficient (U) is applied to measure the performance (Brockfeld et al., 2005; Ahmed, 1999), which is defined as follows:

$$U = \frac{\sqrt{\frac{1}{N} \sum_i (v_{ave}^{5i} - v_{simu}^{5i})^2}}{\sqrt{\frac{1}{N} \sum_i (v_{ave}^{5i})^2 + \frac{1}{N} \sum_i (v_{simu}^{5i})^2}} \quad (6)$$

1 where v_{simu}^{5i} is the i th speed of the simulation data at station 5. v_{ave}^{5i} is the i th lane average speed of the empirical data
 2 calculated by Equation (5) at station 5. N is the number of the data points. The value of U is always in the range
 3 between 0 and 1 with $U = 0$ implying a perfect fitness. Related to Theil's U , the bias (U^M) and the variance (U^S)
 4 are often applied:

$$5 \quad U^M = \frac{(\mu_{v_{ave}^5} - \mu_{v_{simu}^5})^2}{\frac{1}{N} \sum_i (v_{ave}^{5i} - v_{simu}^{5i})^2} \quad (7)$$

$$6 \quad U^S = \frac{(\sigma_{v_{ave}^5} - \sigma_{v_{simu}^5})^2}{\frac{1}{N} \sum_i (v_{ave}^{5i} - v_{simu}^{5i})^2} \quad (8)$$

7 where $\mu_{v_{ave}^5}$, $\mu_{v_{simu}^5}$, $\sigma_{v_{ave}^5}$ and $\sigma_{v_{simu}^5}$ are the means and standard deviations of the empirical and the simulated speed
 8 series at station 5, respectively. The bias proportion (U^M) reflects the systematic error. The variance proportion (U^S)
 9 indicates how well the fluctuation in the original data is replicated by the simulation. Therefore, lower values (close to
 10 zero) of U^M and U^S are desired.

11

12 5.3. Calibration

13 In contrast to previous works (Brockfeld et al., 2005; Wagner et al., 2010), the automated calibration methods are
 14 not used, since they did not always converge. Moreover, once the cell length L_{cell} is determined, the parameters of
 15 the NH model can be calibrated in a straightforward way. The maximum speed v_{max} can be taken as the maximum of
 16 the empirical data if there are periods of free flow (otherwise, it cannot be estimated). Through the average free flow
 17 speed v_{free}^{ave} , the randomization probability p_c is calculated by $v_{free}^{ave} = v_{max} - p_c$. The randomization probability p_b
 18 can be estimated by $v_g \approx -(1 - p_b) / k_{max}$ if the downstream propagation speed of the wide moving jam v_g is
 19 determined, where k_{max} is the density inside the jam. Rehborn et al. (2011) have discussed several methods to
 20 measure v_g and found it inside the interval [-18, -10] km/h while Treiber et al. (2010) give the interval [-20, -15] km/h.
 21 The parameter t_c affects the emergence of wide moving jams. Given a fixed probability p_b , a larger t_c increases the
 22 probability that congested traffic is in the synchronized state, i.e., it reduces the probability of an S→J transition
 23 (Jiang and Wu, 2003). The parameter g_{safety} is not smaller than the deceleration b_{defens} to keep safety. It can be
 24 adjusted after other parameters are determined. Furthermore, we found it is best not to unnecessarily change the value
 25 of randomization probability p_a . Since the vehicle length L_{veh} is about 7.5m, it can be identified after L_{cell} is given.
 26 Thus, only L_{cell} , T and b_{defens} are left to be adjusted, which influence the state of the synchronized flow. The trial and
 27 error method is adopted to determine their values.

28 During the simulations, we found that a smaller cell length L_{cell} is needed to make the simulation data more
 29 consistent with the empirical data and $L_{cell}=1m$ is good enough to obtain satisfactory results (cf. Table 4). Since the
 30 maximum speed measured by the detectors is around 20 m/s, we set $v_{max}=20L_{cell}/s$. As the vehicle types and lengths
 31 are unknown, only one type of vehicle of length $L_{veh}=7L_{cell}=7m$ is assumed. The wide moving jams have not been
 32 detected, so p_b and t_c will not be changed from the values of Table 3. Figures 12(b) and (c) visualize the effect of the
 33 calibration procedure. While a simulation with the un-calibrated values (Table 3) results in a poor fit (Fig. 12(b)), we

obtain a good agreement after calibration (Fig. 12(c)). Specifically, using the un-calibrated values, we always obtain free flow which means the synchronized flow in front is underestimated. Thus, we need to increase the values of T and b_{defens} .

The calibrated model parameters and the resulting U values are given in Tables 4 and the first column of Table 5, respectively. Due to the stochastic nature of the model, separate runs of simulation with the optimal model parameters lead to different U values. Nevertheless, we found that repeated runs only lead to slightly different U values. All the simulated speed series show a good agreement with the empirical data, see Fig.12(c), which is the result of one run. Table 6 is the average time headway of the I-80 trajectory data of NGSIM collected at the location between station 7 and 8 on April 13, 2005. The average time headway varies between 1.78 s to 13.13 s in Tab.6. Since the average time headway of our calibration result is 4.5s, the value of T is reasonable.

Table 4

Model parameters of NH model calibrated to the I-80-North detector data of 07. April 2005 by minimizing Theil's U.

Parameters	L_{cell}	L_{veh}	v_{max}	T	b_{defens}	p_a	p_b	p_c	g_{safety}	t_c
Units	m	L_{cell}	L_{cell}/s	s	L_{cell}/s^2	-	-	-	L_{cell}	s
Value	1	7	21	5.2	2	0.95	0.55	0.1	4	8

Table 5

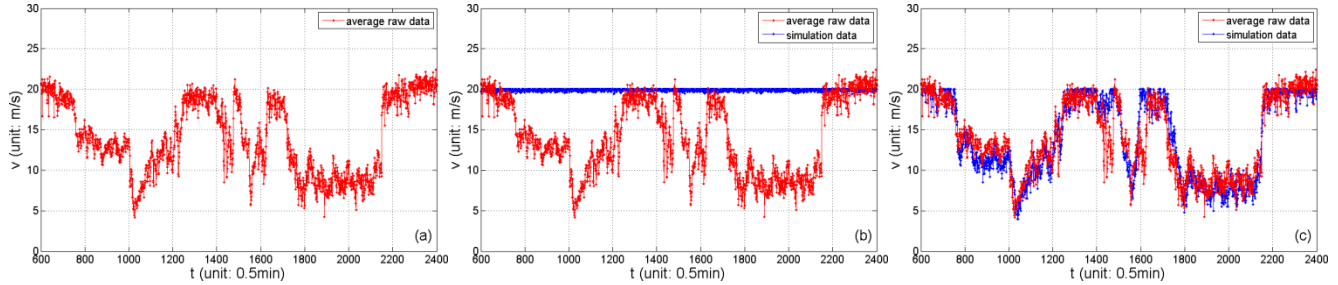
Calibration (07. April 2005) and validation errors (other days) corresponding to Fig.12-17.

Day	07 Apr	08 Apr	11 Apr	12 Apr	13 Apr	14Apr
U	0.0647	0.0689	0.0503	0.0485	0.0471	0.0653
U^M	0.0362	0.1184	0.0182	0.0003	0.0006	0.0167
U^S	0.0125	0.0218	0.0218	0.0036	0.0390	0.0343

Table 6

Average time headways (unit: s) by time period and lane (in seconds) of I-80 trajectories data.

Time period (minutes)	lane				
	1	2	3	4	5
3:58:55-4:00	4.92	4	7.06	3.66	4.1
4:00-4:05	2.4	2.69	2.7	2.89	2.95
4:05-4:10	2.48	3.38	4.84	3.83	3.64
4:10-4:15	2.36	2.99	3.49	4.7	3.81
4:15-4:15:37	2.06	2.84	3.07	3.75	4.61
4:59:27-5:00	2.54	2.34	2.34	2.53	2.76
5:00-5:05	2.39	3.05	3.82	5.51	3.09
5:05-5:10	2.13	3.73	3.93	4.15	4.03
5:10-5:15	2.3	7.41	6.45	10.09	8.04
5:15-5:15:47	1.87	3.96	3.73	2.88	3.32
5:12:45-5:15	1.78	3.16	4.01	6.05	5.16
5:15-5:20	2.35	5.74	4.57	3.97	3.14
5:20-5:25	2.31	6.67	5.18	6.09	6.75
5:25-5:30	2.3	7.37	8.33	7.34	7.02
5:30-5:32:14	2.2	7.5	8.66	8.58	13.13

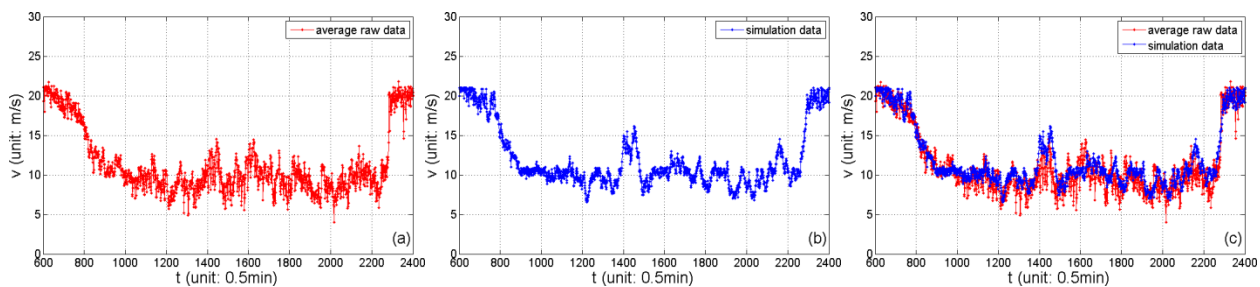


1
2 **Fig.12.** Time series of speed at Station 5 on Thu, 07 Apr 2005. (a) is the lane average speed series calculated by Equation (5). (b, c) are
3 the comparisons between the data in (a) with the simulation speed series. (b) is obtained by the model with the parameter set table 3 with
4 the revised cell length $L_{cell}=1m$, maximum speed $v_{max}=20L_{cell}/s=20m/s$ and vehicle length $L_{veh}=7L_{cell}=7m$. (c) is obtained by the model
5 with the parameter set Table 4.
6

7 5.4. Validations

8 In order to study the robustness of the calibrated parameters, we cross-validate the model by the data collected on
9 other different days. All results are described in Tab.5 and the result of Fri, 08 Apr 2005 is shown in Fig.13. The
10 model can capture the empirical traffic dynamics accurately on all days (08-12 Apr). All validation results are
11 acceptable and better than that of the models tested by Brockfeld et al. (2005) and Wagner et al. (2010). They have
12 tested many microscopic and macroscopic models on the same location with the same detectors at the opposed
13 direction. The models include the NaSch model (Nagel and Schreckenberg, 1992), Newell's model (Newell, 2002),
14 the OV model (Bando et al., 1995), the Cell Transmission model (Daganzo, 1994), Gipps's model (Gipps, 1981), the
15 SK model (Krauss et al., 1997), the IDM (Treiber et al., 2000), and the macroscopic model proposed by Aw and
16 Rascole (2000). The best model tested by Wagner et al. (2010) is the SK model, which was also tested by Brockfeld et
17 al. (2005). The calibration and validation errors (U values) presented by Brockfeld et al. (2005) are in the range of
18 0.14 to 0.16, 0.14 to 0.23, respectively.

19 Moreover, it should be noted that our simulations are based on the homogeneous traffic and the heterogeneity is
20 not considered, while real traffic flow is heterogeneous. Thus, the validation results mean that the real heterogeneous
21 traffic can be simulated by the homogeneous traffic of NH model, which is highlighted as the one of the prominent
22 advantages of the models within the three-phase theory (Kerner, 2012).
23



24 **Fig.13.** Time series of speed at Station 5 on Fri, 08 Apr 2005.(a) is the lane average speed series calculated by Equation (5). (b) is the
25 simulation speed series. (c) is the comparisons between the data in (a) with the data in (b).
26
27

28 6. Conclusion

29 The fundamental diagram approach assumes the existence of a unique space gap vs. speed relationship, while the
30 three-phase theory presumes that, within a certain range, drivers can make arbitrary choices of the space gap. In order
31 to determine whether the unique space-gap-speed relationship exists, the US-101 trajectory datasets of NGSIM are
32 analyzed. Results showed the following findings in 82% of the cases: (1) a linear relationship between actual space

1 gap and speed can be identified when the speed difference between vehicles is approximately zero; (2) vehicles
 2 accelerate or decelerate around the desired space gap most of the time. To explain these phenomena, an assumption
 3 and a new cellular automaton model (NH model) are proposed such that, for homogeneous congested traffic flow in
 4 the noiseless limit, the space gap will oscillate around the desired space gap rather than keeping it exactly. This
 5 provides a possible dynamical explanation for the observed variation of the gaps for a given speed.

6 Two parts of simulations are conducted. In the first part, simulations on both a circular road and an open road
 7 with an on-ramp were carried out for NH model. Results obtained under the periodic conditions show that the NH
 8 model could produce the synchronized flow and two kinds of phase transitions which can be identified as F→S and
 9 S→J transitions. Results obtained from an open road with an on-ramp show that multiple congested patterns observed
 10 by simulating models of three-phase theory can be well reproduced by the NH model. In the second part, the NH
 11 model has been calibrated and validated by the I-80 detector datasets of NGSIM. Results show that the empirical data
 12 can be well reproduced and the validation errors are smaller than that of previous studies.

14 Acknowledgements:

15 The authors wish to thank NGSIM for supplying the empirical data used in this article. Tian sincerely thanks for
 16 the help of Guojun Jiang and Yang Xu to deal with the empirical data. This work is supported by the National Natural
 17 Science Foundation of China (Grant Nos. 71271150, 71101102, 71222101, 71131001), and the 973 Program (No.
 18 2012CB725400).

20 Appendix: The three-phase theory

21 A.1. Congested traffic phases

22 In three-phase theory, congested traffic has been divided into the synchronized flow and wide moving jam phases,
 23 which are defined through empirical criteria [S] and [J]:

24 Wide moving jams [J]: A wide moving jam is a moving jam that maintains the mean speed of the downstream jam
 25 front, even when the jam propagates through other traffic phases or bottlenecks. Within the downstream front of the
 26 wide moving jam, vehicles accelerate from the standstill inside the jam to free flow. Within the wide moving jam, the
 27 vehicles are almost in a standstill or if they are moving, their speeds are very low. Within the upstream front of the
 28 wide moving jam vehicles must slow down to the speed within the jam. Generally, if the width of a moving jam (in
 29 the longitudinal direction) considerably exceeds the width of the jam fronts, one could call it a wide moving jam.

30 The synchronized flow phase [S]: In contrast with the wide moving jam phase, the downstream front of the
 31 synchronized flow phase does not exhibit the wide moving jam characteristic feature; in particular, the downstream
 32 front of the synchronized flow phase is often fixed at a bottleneck. In synchronized flow, the average speed of vehicles
 33 is noticeably lower and the density of vehicles is noticeably higher than the corresponding values in free traffic at the
 34 same flux of vehicles.

35 The criterion [J] could be explained by a flow interruption effect within a wide moving jam that occurs when
 36 vehicles are in a standstill or move with negligible low speed within the jam. A sufficient criterion for this flow
 37 interruption effect is:

$$38 \quad T_{max} \gg T_{del}^{(ac)} \quad (9)$$

39 where T_{max} is the maximum time headway between two vehicles within the jam and $T_{del}^{(ac)}$ is the mean time
 40 delay in vehicle acceleration at the downstream jam front from a standstill state within the jam. In a hypothetical case,
 41 when all vehicles within a moving jam do not move, the criterion for this flow interruption effect is:

$$T_j \gg T_{del}^{(ac)} \quad (10)$$

where T_j is the jam duration, i.e. the time interval between the upstream and downstream jam fronts passing a detector location.

Condition (9) indicates that vehicles inside the moving jam is at least once in a stop during a large time interval compared with the mean time delay in vehicles acceleration from standstill at the downstream front. Under condition (9), there are at least several vehicles within the jam that are in a standstill or if they are still moving, it is only with a negligible low speed in comparison with the speed in the jam inflow and outflow. These vehicles could separate vehicles accelerating at the downstream jam front from vehicles decelerating at the upstream jam front. Therefore the jam inflow has no influence on the jam outflow, and the jam outflow only depends on the vehicles that accelerating from standstill at the downstream front. Thus, the traffic flow interruption effect can be used as a criterion to distinguish the synchronized flow from wide moving jams in single vehicle data.

A.2. The fundamental hypothesis of the three-phase traffic theory

The fundamental hypothesis of the three-phase theory is as follows: the hypothetical steady states of the synchronized flow cover a two-dimensional region in the flow-density plane, i.e., there is no fundamental diagram of traffic flow in this theory, Fig. A.1. The steady state of synchronized flow is a hypothetical state of synchronized flow of identical vehicles and drivers in which all vehicles move with the same time independent speed and have the same space gaps, i.e., this synchronized flow is homogeneous in time and space. This fundamental hypothesis assumes that the driver can make an arbitrary choice in the space gap to the preceding vehicle within a finite range of space gaps at a given speed in the steady states of synchronized flow.

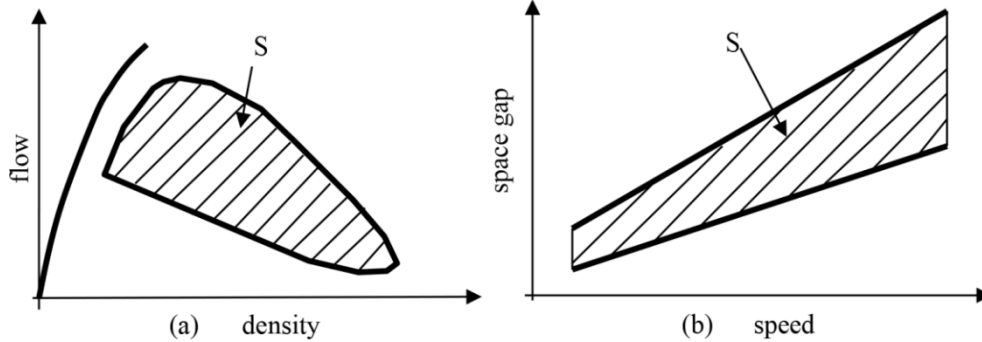


Fig. A.1. Fundamental hypothesis of three-phase traffic theory: (a) Qualitative representation of free flow states (F) and 2D steady states of synchronized flow (dashed region S) on a multi-lane road in the flow-density plane. (b) A part of the 2D steady states of synchronized flow shown in (a) in the space-gap-speed plane (dashed region S) (Kerner, 2009).

A.3. Phase transitions

In three-phase traffic theory, traffic breakdown is a phase transition from free flow to synchronized flow (F→S transition). Wide moving jams can occur spontaneously in synchronized flow only (S→J transition), i.e. due to a sequence F→S→J transitions. In real traffic, a fluctuation, whose amplitude exceeds the critical amplitude, occurring in the vicinity of the bottlenecks in the free traffic flow, will lead to the transition from free flow to synchronized flow (F→S transition). Jams emerge in the synchronized flow, i.e. narrow moving jams, who spontaneously emerge in the synchronized flow, move and grow in the upstream direction. Finally, these narrow moving jams (or a part of them) transform into wide moving jams (S→J transition).

F→S transition: if before traffic breakdown occurs at a bottleneck, there is free flow at the bottleneck as well as

1 upstream and downstream in a neighborhood of the bottleneck, then the $F \rightarrow S$ transition is called as spontaneous $F \rightarrow S$
2 transition. On the other hand, if the $F \rightarrow S$ transition is induced by the propagation of a spatiotemporal congested traffic
3 pattern, then the $F \rightarrow S$ transition is called as the induced $F \rightarrow S$ transition.

4 $S \rightarrow J$ transition: In empirical observations, $S \rightarrow J$ transition developments is associated with a pinch effect, which
5 is the spontaneous emergence of growing narrow moving jams in the synchronized flow occurring within the
6 associated pinch region of synchronized flow. If the growth of a nucleus required for moving jam emergence appears
7 within the synchronized flow, the $S \rightarrow J$ transition is called as the spontaneous $S \rightarrow J$ transition. Just like the $F \rightarrow S$
8 transition, there also exists the induced $S \rightarrow J$ transition.

10 *A.4. Patterns at bottlenecks*

11 Empirical observations show that there are two main types of congested patterns at an isolated bottleneck:

12 The General Patterns (GPs): After the synchronized flow occurs upstream of the bottleneck, the wide moving
13 jams continuously emerge in that synchronized flow and propagate upstream, and then this congested pattern is often
14 called as the General Patterns (GP). However, if the wide moving jams discontinuous emerge on the road, there will
15 be just one or few wide moving jams appearing in that synchronized flow, then this congested pattern is often called
16 as the dissolving General Patterns (DGP).

17 The Synchronized Patterns (SPs): If there only is synchronized flow upstream of the bottleneck, no wide moving
18 jams emerge in the synchronized flow, and then this congested pattern is often called as the Synchronized Patterns.
19 And as a result of the $F \rightarrow S$ transition, various synchronized flow patterns can occurs at the bottleneck, such as the
20 widening synchronized pattern (WSP), local synchronized pattern (LSP), moving synchronized pattern (MSP), and
21 alternating synchronized pattern (ASP).

23 *A.5. Models based on the three-phase traffic theory*

24 In 2002, Kerner and Klenov (2002) proposed the KK car following model, which is able to show all known
25 microscopic and macroscopic features of traffic breakdown, synchronized flow and congested patterns for the first
26 time. Later, the one-lane KKW CA model and two-lane KKS CA model (Kerner et al., 2002, 2011) are proposed. The
27 main idea of above models is the speed adaptation effect within the synchronized distance. The vehicle tends to adjust
28 its speed to the preceding vehicle as long as it is safe. Lee et al. (2004) developed the CA model mainly considering
29 mechanical restriction versus human overreaction. This model could exhibit some features of SPs and GPs. The Brake
30 Light CA Model (BLM, Knospe et al., 2000) and its variants (Comfortable Driving Models (CDMs)) (Jiang and Wu,
31 2003, 2005; Tian et al., 2009) have considered the brakelight effect, i.e., the simulated drivers adopt a more defensive
32 driving strategy if the brake lights of the preceding vehicle are on, i.e., if this vehicle decelerates. The CDMs are based
33 on the BLM. Simulation results of CDMs show SPs and GPs as well as the diagram of congested patterns at an
34 on-ramp bottleneck postulated in the three-phase traffic theory. The CA model by Gao et al. (2007, 2009) mainly
35 assumes that randomization depends on speed difference. It is pointed out that this model is equivalent to a
36 combination of the KKW model and the NaSch model. The car following model proposed by Davis (2004)
37 incorporates the reaction delay into the optimal car following model, which can describe the $F \rightarrow S$ transition. The car
38 following model by Kerner and Klenov (2006) considered different time delays on driver acceleration associated with
39 driver behavior in various local driving situations, which can show spatiotemporal congested patterns that are
40 adequate with empirical results. He et al. (2010) proposed a deterministic car-following model based on a
41 multi-branch fundamental diagram with each branch representing a particular category of driving style. Traffic
42 breakdown and some observed spatio-temporal patterns at on-ramp vicinity are reproduced.

43 In order to emphasize the significance of the two-dimensional steady states of synchronized flow, Kerner and

1 Klenov (2006) proposed the Speed Adaption Models (SAMs) in the framework of fundamental diagram approach.
2 The basic hypothesis of SAMs is the double Z-characteristic for the sequence of phase transitions from free flow to
3 synchronized flow to wide moving jams ($F \rightarrow S \rightarrow J$ transitions). Based on this hypothesis, SAMs can reproduce both
4 the traffic breakdown and the emergence of wide moving jams in synchronized flow as found in empirical
5 observations. However, SAMs are not able to reproduce the local synchronized patterns (LSPs) consistent with
6 empirical results as well as some of empirical features of synchronized flow between wide moving jams within
7 general patterns (GPs). Kerner et al. attribute these drawbacks of SAMs to the lacking of the two-dimensional steady
8 states of synchronized flow.
9

10 References:

- 11 Ahmed, K. I., 1999. Modeling drivers' acceleration and lane changing behavior. Ph. D. thesis, Massachusetts Institute of
12 Technology.
- 13 Aw, A., Rascle, M., 2000. Resurrection of "second order" models of traffic flow. SIAM journal on applied mathematics 60(3),
14 916-938.
- 15 Bando, M., Hasebe, K., Nakayama, A., Shibata, A., Sugiyama, Y., 1995. Dynamical model of traffic congestion and numerical
16 simulation. Physical Review E 51, 1035-1042.
- 17 Bham, G. H., Benekohal, R. F., 2004. A high fidelity traffic simulation model based on cellular automata and car-following
18 concepts. Transportation Research Part C: Emerging Technologies 12(1), 1-32.
- 19 Brockfeld, E., Kühne, R. D., Wagner, P., 2005. Calibration and validation of microscopic models of traffic flow. Transportation
20 Research Record: Journal of the Transportation Research Board 1934(1), 179-187.
- 21 Chowdhury, D., Santen, L., Schadschneider, A., 2000. Statistical physics of vehicular traffic and some related systems. Physics
22 Reports 329(4), 199-329.
- 23 Daganzo, C. F., 1994. The cell transmission model: A dynamic representation of highway traffic consistent with the hydrodynamic
24 theory. Transportation Research Part B: Methodological 28(4), 269-287.
- 25 Davis, L., 2004. Effect of adaptive cruise control systems on traffic flow. Physical Review E 69(6), 066110.
- 26 Gao, K., Jiang, R., Hu, S.-X., Wang, B.-H., Wu, Q.-S., 2007. Cellular-automaton model with velocity adaptation in the framework
27 of Kerner's three-phase traffic theory. Physical Review E 76(2), 026105.
- 28 Gao, K., Jiang, R., Wang, B.-H., Wu, Q.-S., 2009. Discontinuous transition from free flow to synchronized flow induced by
29 short-range interaction between vehicles in a three-phase traffic flow model. Physica A: Statistical Mechanics and its
30 Applications 388(15), 3233-3243.
- 31 Gipps, P. G., 1981. A behavioural car-following model for computer simulation. Transportation Research Part B: Methodological
32 15(2), 105-111.
- 33 Greenshields, B. D., Bibbins, J., Channing, W., Miller, H., 1935. A study of traffic capacity, Highway research board proceedings.
- 34 Haight, F. A., 1963. Mathematical Theories of Traffic Flow. Academic Press, New York.
- 35 He, S., Guan, W., Song, L., 2010. Explaining traffic patterns at on-ramp vicinity by a driver perception model in the framework of
36 three-phase traffic theory. Physica A: Statistical Mechanics and its Applications 389(4), 825-836.
- 37 Helbing, D., 2001. Traffic and related self-driven many-particle systems. Reviews of modern physics 73(4), 1067.
- 38 Herman, R., Montroll, E. W., Potts, R. B., Rothery, R. W., 1959. Traffic dynamics: analysis of stability in car following. Operations
39 Research 7(1), 86-106.
- 40 Jia, B., Gao, Z.-y., Ke-ping, L., Li, X.-g., 2007. Models and Simulations of Traffic System Based on the Theory of Cellular
41 Automaton. Science, Beijing.
- 42 Jiang, R., Wu, Q.-S., 2003. Cellular automata models for synchronized traffic flow. Journal of Physics A: Mathematical and
43 General 36(2), 381.
- 44 Jiang, R., Wu, Q., 2005. First order phase transition from free flow to synchronized flow in a cellular automata model. The
45 European Physical Journal B-Condensed Matter and Complex Systems 46(4), 581-584.
- 46 Kerner, B. S., 2004. The physics of traffic: empirical freeway pattern features, engineering applications, and theory. Springer
47 Verlag.
- 48 Kerner, B. S., 2009. Introduction to modern traffic flow theory and control: the long road to three-phase traffic theory. Springer.
- 49 Kerner, B. S., 2012. Complexity of spatiotemporal traffic phenomena in flow of identical drivers: Explanation based on
50 fundamental hypothesis of three-phase theory. Physical Review E 85(3), 036110.
- 51 Kerner, B. S., Klenov, S. L., 2002. A microscopic model for phase transitions in traffic flow. Journal of Physics A: Mathematical

1 and General 35(3), L31.

2 Kerner, B. S., Klenov, S. L., 2003. Microscopic theory of spatial-temporal congested traffic patterns at highway bottlenecks.
3 Physical Review E 68(3), 036130.

4 Kerner, B. S., Klenov, S. L., 2006. Deterministic microscopic three-phase traffic flow models. Journal of Physics A: Mathematical
5 and General 39(8), 1775.

6 Kerner, B. S., Klenov, S. L., Schreckenberg, M., 2011. Simple cellular automaton model for traffic breakdown, highway capacity,
7 and synchronized flow. Physical Review E 84(4), 046110.

8 Kerner, B. S., Klenov, S. L., Wolf, D. E., 2002. Cellular automata approach to three-phase traffic theory. Journal of Physics A:
9 Mathematical and General 35(47), 9971.

10 Kesting, A., Treiber, M., 2008. How reaction time, update time, and adaptation time influence the stability of traffic flow. Computer
11 - Aided Civil and Infrastructure Engineering 23(2), 125-137.

12 Knospé, W., Santen, L., Schadschneider, A., Schreckenberg, M., 2000. Towards a realistic microscopic description of highway
13 traffic. Journal of Physics A: Mathematical and general 33(48), L477.

14 Krauss, S., Wagner, P., Gawron, C., 1997. Metastable states in a microscopic model of traffic flow. Physical Review E 55(5),
15 5597-5602.

16 Lee, H. K., Barlovic, R., Schreckenberg, M., Kim, D., 2004. Mechanical restriction versus human overreaction triggering congested
17 traffic states. Physical Review Letters 92(23), 238702.

18 Leutzbach, W., 1987. Introduction to the theory of traffic flow.

19 Lighthill, M. J., Whitham, G. B., 1955. On kinematic waves. II. A theory of traffic flow on long crowded roads. Proceedings of the
20 Royal Society of London. Series A. Mathematical and Physical Sciences 229(1178), 317-345.

21 Nagatani, T., 2002. The physics of traffic jams. Reports on progress in physics 65(9), 1331.

22 Nagel, K., Schreckenberg, M., 1992. A cellular automaton model for freeway traffic. Journal de Physique I 2(12), 2221-2229.

23 Neubert, L., Santen, L., Schadschneider, A., Schreckenberg, M., 1999. Single-vehicle data of highway traffic: A statistical analysis.
24 Physical Review E 60(6), 6480.

25 Newell, G. F., 2002. A simplified car-following theory: a lower order model. Transportation Research Part B: Methodological 36(3),
26 195-205.

27 NGSIM, 2006. Next generation simulation.<<http://ngsim.fhwa.dot.gov/>>.

28 Payne, H. J., 1979. FREFLO: A macroscopic simulation model of freeway traffic. Transportation Research Record (722).

29 Rehborn, H., Klenov, S. L., Palmer, J., 2011. An empirical study of common traffic congestion features based on traffic data
30 measured in the USA, the UK, and Germany. Physica A: Statistical Mechanics and its Applications 390(23), 4466-4485.

31 Richards, P. I., 1956. Shock waves on the highway. Operations Research 4(1), 42-51.

32 Tang, T.-Q., Huang, H.-J., Gao, Z.-Y., 2005. Stability of the car-following model on two lanes. Physical Review E 72(6), 066124.

33 Tian, J.-f., Jia, B., Li, X.-g., Jiang, R., Zhao, X.-m., Gao, Z.-y., 2009. Synchronized traffic flow simulating with cellular automata
34 model. Physica A: Statistical Mechanics and its Applications 388(23), 4827-4837.

35 Tian, J.-f., Yuan, Z.-z., Jia, B., Fan, H.-q., Wang, T., 2012a. Cellular automaton model in the fundamental diagram approach
36 reproducing the synchronized outflow of wide moving jams. Physics Letters A.

37 Tian, J.-f., Yuan, Z.-z., Treiber, M., Jia, B., Zhang, W.-y., 2012b. Cellular automaton model within the fundamental-diagram
38 approach reproducing some findings of the three-phase theory. Physica A: Statistical Mechanics and its Applications 391(11),
39 3129-3139.

40 Treiber, M., Hennecke, A., Helbing, D., 2000. Congested traffic states in empirical observations and microscopic simulations.
41 Physical Review E 62(2), 1805.

42 Treiber, M., Kesting, A., Helbing, D., 2006. Understanding widely scattered traffic flows, the capacity drop, and platoons as effects
43 of variance-driven time gaps. Physical Review E 74(1), 016123.

44 Treiber, M., Kesting, A., Helbing, D., 2010. Three-phase traffic theory and two-phase models with a fundamental diagram in the
45 light of empirical stylized facts. Transportation Research Part B: Methodological 44(8), 983-1000.

46 Treiber, M., Kesting, A., 2013. Traffic Flow Dynamics. Springer.

47 Wagner, P., 2010. Fluid-dynamical and microscopic description of traffic flow: a data-driven comparison. Philosophical
48 Transactions of the Royal Society A: Mathematical, Physical and Engineering Sciences 368(1928), 4481-4495.

49 Wagner, P., 2012. Analyzing fluctuations in car-following. Transportation Research Part B: Methodological 46(10), 1384-1392.

50 Whitham, G. B., 2011. Linear and nonlinear waves. Wiley-interscience.